analytical chemistry

pubs.acs.org/ac Article

Pore Size Adjustment Strategy for the Fabrication of Molecularly Imprinted Covalent Organic Framework Nanospheres at Room Temperature for Selective Extraction of Zearalenone in Cereal Samples

Hao-Ze Li, Cheng Yang, Hai-Long Qian, Shu-Ting Xu, and Xiu-Ping Yan*

Cite This: *Anal. Chem.* 2024, 96, 3561−3568 Read Online

ACCESS | Metrics & More | Article Recommendations | Supporting Information

ABSTRACT: Covalent organic frameworks (COFs) are attractive adsorbents for sample pretreatment due to their unique structure and properties. However, the selectivity of COFs for the extraction of hazardous compounds is still limited due to the lack of specific interactions between COFs and targets. Herein, we report a pore size adjustment strategy for room-temperature synthesis of molecularly imprinted COF (MICOF) for selective extraction of zearalenone (ZEN) in complex food samples. The three-dimensional building block tetra(4-aminophenyl) methane was used as a functional monomer, while dialdehyde monomers with different numbers of benzene ring were used to adjust the pore size of MICOF to match with the size of ZEN molecules. The prepared MICOF gave the largest adsorption capacity of 177.2 mg g^{-1} and the highest imprinting factor of 10.1 for ZEN so far. MICOF was used as the adsorbent for dispersed solid-phase extraction in combination with high-performance liquid chromatography for the determination of trace ZEN in cereals. The high selectivity of the developed method allows simple aqueous standard calibration for the matrix effect-free determination of ZEN in food samples. The limit of detection and the recoveries of the developed method were 0.21 $\mu g\ kg^{-1}$ and 93.7−101.4%, respectively. The precision for the determination of ZEN was less than 3.8% (RSD, $n = 6$). The developed method is promising for the selective determination of ZEN in complex matrices.

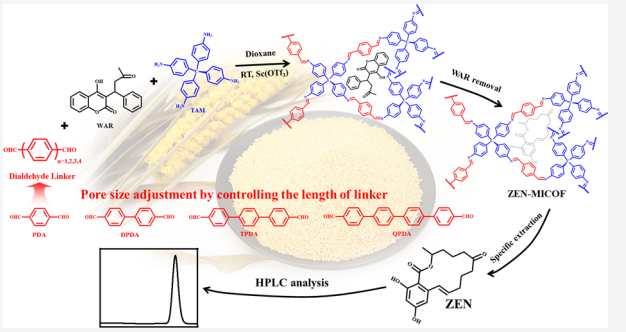

INTRODUCTION

Nearly 25% of cereal products contain mycotoxins, posing a potential risk for human health.[1] Zearalenone (ZEN) is one of the most common Fusarium mycotoxins and might cause carcinogenicity, hepatotoxicity, genotoxicity, and immunosuppression.[2] ZEN is hard to degrade or remove during food processing due to its high thermal stability.[3] According to the European Food Safety Authority, the tolerable daily intake for ZEN should not exceed 0.25 $\mu g\ kg^{-1}$ of body weight.[4] The maximum tolerable content (20−400 $\mu g\ kg^{-1}$) of ZEN in food products for human is specified by the European Commission,[5] while the limit of ZEN in wheat and maize is 60 $\mu g\ kg^{-1}$ in Chinese food safety standards (GB 2761-2017).[6] Therefore, development of analytical methods for selective and precise determination of trace ZEN in complex food samples is of great significance in food safety.

Various methods have been reported for the determination of ZEN in food samples so far. Commonly used methods are high-performance liquid chromatography (HPLC) equipped with a diode array detector (DAD),[6] fluorescence detection (FLD),[7] mass spectrometry (MS),[8] gas chromatography−mass spectrometry (GC−MS),[9] electrochemical assay,[10] and enzyme-linked immunosorbent assay (ELISA).[11] In these analytical methods, sample pretreatment is a critical step for the analysis of complex food samples. Until now, various pretreatment methods, including solid-phase extraction (SPE),[12] dispersed solid-phase extraction (DSPE),[13] liquid−liquid extraction (LLE),[14] and immunoaffinity column (IAC) extraction,[15] have been used before ZEN determination. Although IAC gives better selectivity, it is expensive and not reuseable.[16] DSPE has advantages such as simple operation, easy regeneration, and less solvent consumption.[17] Some DSPE adsorbents like zirconia,[18] poly(dopamine),[19] and nanographene[20] were introduced in the detection of ZEN. However, their selectivity for the extraction of ZEN is still insufficient. Therefore, the development of highly selective

Received: December 4, 2023
Revised: January 16, 2024
Accepted: February 8, 2024
Published: February 19, 2024

Downloaded via JIANGNAN UNIV on March 11, 2024 at 09:56:37 (UTC).
See https://pubs.acs.org/sharingguidelines for options on how to legitimately share published articles.

ACS Publications © 2024 American Chemical Society

https://doi.org/10.1021/acs.analchem.3c05512
Anal. Chem. 2024, 96, 3561−3568

adsorbents for DSPE is highly imperative for ZEN determination.

Molecular imprinting polymers (MIPs) are attractive adsorbents for selective extraction. MIPs are usually prepared via the polymerization of functional monomer and cross-linking agent based on the interaction between functional monomer and template.[21] The removal of template from MIPs leaves the imprinted cavity which can recognize the template molecules specifically.[22,23] MIPs have been used for the extraction of ZEN from food samples.[6,16,24] However, the MIPs prepared by traditional methods are composed of a flexible skeleton of carbon−carbon single bonds, which makes them prone to distortion and aggregation into dense structures.[25] As a result, conventional MIPs suffer from insufficient adsorption capacity and specificity for the extraction of ZEN in complex samples.

Covalent organic frameworks (COFs) are a class of porous crystalline polymers.[26] COFs have been widely used in adsorption[27] and sample pretreatment[28] because of their advantages such as low density, stable structure, uniform pore, and easy postmodification. COFs have also been applied for sample pretreatment before ZEN determination.[29] However, COFs themselves still cannot meet the requirement for the selective extraction of target molecules due to the lack of specific interactions between COFs and targets.[25]

Recently, MIPs have been integrated with COFs to improve the selectivity in sample pretreatment. Molecule imprinted COFs (MICOFs) were synthesized to achieve selective extraction of sterigmatocystin from cereals,[30] cyano pyrethroids from plants,[31] and cyanidin-3-oglucoside from plant samples.[25,32] However, no work on the preparation of ZEN-imprinted COFs has been reported before. Moreover, previous MICOFs are mainly based on two-dimensional (2D) COFs. Compared to 2D COFs, three-dimensional (3D) COFs give more complicated pore structures (interpenetrated channels), which are beneficial to adsorption and guest incorporation.[33] In addition, the more flexible structures of 3D COFs due to the freedom orientation of building blocks and lack of $\pi-\pi$ stacking give more advantages for constructing MICOF.[34] Furthermore, no work on the effect of pore size on the imprinting effect of MICOFs has been reported so far.

Here, we propose a pore size adjustment strategy for room-temperature fabrication of ZEN-imprinted 3D COF for selective extraction of trace ZEN in complex food samples. Three-dimensional building block tetra(4-aminophenyl) methane (TAM) and warfarin (WAR) were used as the functional monomer and the pseudo-template for ZEN, while dialdehyde monomers with different numbers of benzene ring were explored to adjust the pore size of MICOF to match with the size of ZEN molecule. The prepared MICOF gave the largest adsorption capacity and the highest selectivity for ZEN reported so far. Furthermore, a selective MICOF based DSPE method was developed for HPLC determination of ZEN in cereal samples. The high selectivity of the developed method allows simple aqueous standard calibration for matrix-effect-free determination of ZEN in food samples.

EXPERIMENTAL SECTION

Chemicals and Reagents. Please see the Supporting Information.

Synthesis of MICOF. TAM (19.0 mg, 0.05 mmol), 1,4-phthalaldehyde (PDA, 13.4 mg, 0.1 mmol), and WAR (7.7 mg, 0.025 mmol) were dissolved into 5 mL of 1,4-dioxane (DOX) via sonication, followed by standing for 1 h. Afterward, the mixture was catalyzed by dropping $Sc(OTf)_3$ (6 mg in 200 μL of DOX) under sonication and standing at room temperature for 24 h. Subsequently, the precipitate was washed with tetrahydrofuran (THF), and the pseudo-template WAR was eluted with a mixture of methanol (MeOH)/acetic acid (HAc) (9:1, v/v) until no template was detected by UV−vis spectrophotometry. The product was washed to be neutral with MeOH and dried under vacuum at 60 °C for 12 h to yield yellow powder. The nonimprinted COF (NICOF) was prepared in parallel to MICOF but in the absence of the pseudo-template.

Instrumentation. The determination of ZEN was performed on e2695 HPLC equipped with a 2475 FLR detector (Waters, U.S.A.). All separations were carried out on an XBridege C18 column (5 μm, 4.6 mm × 250 mm) at 30 °C. ACN/H_2O/MeOH solution (46:46:8, v/v) was used as the mobile phase at 1 mL min^{-1}. The sample volume injected was set to 30 μL. The excitation and emission wavelength for the detector were set at 274 and 440 nm, respectively.

Other instruments for material characterization are given in the Supporting Information.

Adsorption Experiments. In the static adsorption experiments, MICOF or NICOF (2 mg) was added into 2 mL of ZEN solution (initial concentrations 10−500 mg L^{-1}, initial pH 6.2). After 1 h shaking (150 rpm) at room temperature, the mixture was filtered with 0.22 μm filter membrane and the concentration of residual ZEN was measured by HPLC.

To investigate the adsorption kinetics, 10 mg of MICOF or NICOF was added into the ZEN solution (10 mL, initial concentration 10 mg L^{-1}). After shaking at 150 rpm for a certain period (5−120 min), 0.2 mL of the solution was collected, filtered, and then analyzed by HPLC for residual ZEN. The adsorption capacity (q, mg g^{-1}) and imprinting factor (IF) were calculated according to eqs 1 and 2, respectively:

$$q = \frac{C_0 - C_t}{m} V \tag{1}$$

$$\mathrm{IF} = \frac{q_{\mathrm{MICOF}}}{q_{\mathrm{NICOF}}} \tag{2}$$

where C_0 (mg/L) and C_t (mg/L) stand for the initial and final concentrations of ZEN, respectively. m (mg) represents adsorbent mass, and V (mL) is solution volume. q_{MICOF} and q_{NICOF} are the adsorption capacity for MICOF and NICOF, respectively.

To test the selectivity of MICOF for the adsorption of ZEN, three other mycotoxins, including aflatoxin B1(AFB1), patulin (PAT), and deoxynivalenol (DON) were selected for comparison. MICOF or NICOF (2 mg) was added into 2 mL of 10 mg L^{-1} each mycotoxin solution. After 1 h shaking (150 rpm) at room temperature, the mixture was filtered with a 0.22 μm filter membrane, and the concentration of residual mycotoxin was measured by HPLC.

Sample Preparation. Five cereal samples (wheat, rice, maize, millet, and oat) were purchased from the local supermarket. Each cereal sample (10 g) was weighed accurately into a 50 mL centrifuge tube, and 18 mL acetonitrile (ACN), 2 mL ultrapure water, and 1 g NaCl were added to homogenize on a high-speed homogenizer for 3 min, followed by supersonic extraction for 10 min. After that, the extract was

https://doi.org/10.1021/acs.analchem.3c05512
Anal. Chem. 2024, 96, 3561−3568

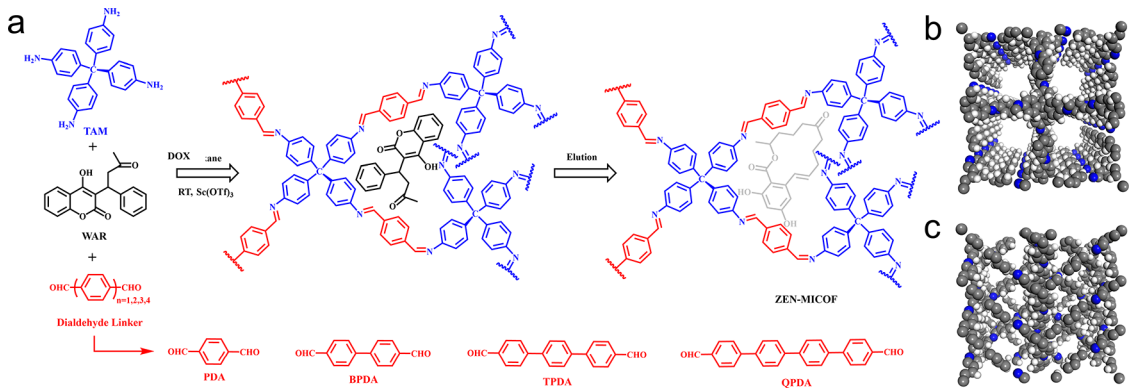

Figure 1. (a) Schematic for the synthesis of MICOF. Top (b) and side (c) views of MICOF.

collected by centrifugation (10,000 rpm for 10 min), dried on a termovap, and redissolved with 1 mL of ACN for further use.

DSPE Procedure. One mL of the above ACN solution was diluted with ultrapure water to 10 mL. MICOF (10 mg) was added into above solution with sonication. The suspension was agitated in a shaker at 180 rpm for 20 min. The MICOF was collected by centrifugation at 10,000 rpm for 10 min, eluted with 1 mL of ACN for 10 min. The mixture was filtered with a 0.22 μm filter membrane, and the concentration of ZEN was measured by HPLC.

RESULTS AND DISCUSSION

Design and Synthesis of MICOF. Figure 1 illustrates the design and preparation of MICOF. 3D COFs with more complicated pore structures, void frameworks and easily accessible adsorption sites (Figure 1a,b) are highly beneficial for adsorption and constructing imprinted sites compared to the uniform one-dimensional channels formed by the tight interlayer stacking in 2D COFs.[33] Typical 3D building unit TAM with symmetrical tetrahedral structure was selected as it can be used to synthesize 3D MICOF with complex interleaved pores and offer $\pi-\pi$ interactions with ZEN. The dialdehyde linkers with different number of benzene rings were used to adjust the pore size of MICOF to better match with the size of ZEN. Pseudo-templates have the advantages of low toxicity, cheapness, and no false positive. WAR was selected as the pseudo-template as it contains a similar partial spatial structure of ZEN. The Schiff-base reaction between TAM and dialdehyde linker was catalyzed by $Sc(OTf)_3$ in the presence of the pseudo-template WAR at room temperature.

The synthesis conditions were investigated in detail to obtain the MICOF with the best imprinting performance. The conditions for the optimization include pseudo-template, dialdehyde linker, solvent, catalyst, and reaction time (Figure S1). The structurally analogous are usually used as pseudo-template molecules to replace the expensive and highly toxic ZEN.[6,7] Three ZEN structure analogues, including WAR, quercetin (QUE), and cyclodo-decanyl-2,4-dihydroxybenzoate (CDHB), were used as pseudo-templates to evaluate the effect of different templates on adsorption performance. The structures after energy minimization of ZEN, WAR, QUE, and CDHB are shown in Figure S2. WAR is closest to ZEN in terms of spatial structure compared to the other two pseudo-templates. Molecular docking results gave the lowest binding energy of QUE (−4.7 kcal mol^{-1}), WAR (−5.2 kcal mol^{-1}), CDHB (−5.3 kcal mol^{-1}), and ZEN (−5.1 kcal mol^{-1}) with the structural unit of MICOF (Figure S3). The lowest binding energy of MICOF with WAR was closest to that of ZEN. The above theoretical studies indicate that WAR is the most suitable pseudo-template. Moreover, the adsorption experimental results also confirmed that the adsorption capacity of MICOF for ZEN was the largest when WAR was used as the pseudo-template (Figure S1a). Therefore, WAR was chosen as the pseudo-template for ZEN. The added amount of template WAR was further optimized. The UV absorption peak of TAM at 300 nm showed a red shift (1−4 nm) as the amount of WAR increased. No further red shift occurred over the mole ratio of TAM/WAR = 2:1 (Figure S4). Consequently, the mole ratio of TAM/WAR = 2:1 was selected for further experiment.

Four dialdehyde linkers (PDA, BPDA, TPDA, and QPDA) with different numbers of benzene rings were used to investigate the influence of the length of dialdehyde linkers on the imprinting effect. Increase of the length of the dialdehyde linker was favorable to nonspecific adsorption but unfavorable to specific adsorption, as reflected by the decrease of IF value (Figure S1b). The pore-size distributions of MICOF-*n* and NICOF-*n* (n is the number of benzene rings in dialdehyde linker) were analyzed based on quenched solid density functional theory (Figures S5−S7). For a certain dialdehyde linker, the pore size of the corresponding MICOF was larger than that of the corresponding NICOF, indicating that the existence of template molecules affected the formation of the pore of the MICOF.[31] However, the pore size of NICOF2−4 was much larger than the molecular size of WAR, and the difference between MICOF and NICOF decreased as the number of benzene rings of dialdehyde linkers increased, leading to the decrease of specific adsorption (less IF). Moreover, the MICOF1−2 with the short dialdehyde length gave larger specific surface area than the corresponding NICOF. In the constructing of MICOF, the presence of template allowed the COF monomers to be arranged in a directional manner, resulting in the imprinted sites and larger specific surface area. The above results indicate that the short dialdehyde length is favorable to the formation of the imprinted sites in the synthesis of MICOF. Thus, PDA was selected as the dialdehyde linker for further experiments.

Careful choice of proper solvent is crucial for the preparation of MICOF due to its important role in the dissolution of monomer and template as well as polymerization process. DOX, THF, ethanol (EtOH), and ACN were used to investigate the influence of the solvent. The template WAR and dialdehyde linker PDA were readily soluble in the above solvents. Furthermore, the monomer TAM was readily soluble

https://doi.org/10.1021/acs.analchem.3c05512
Anal. Chem. 2024, 96, 3561−3568

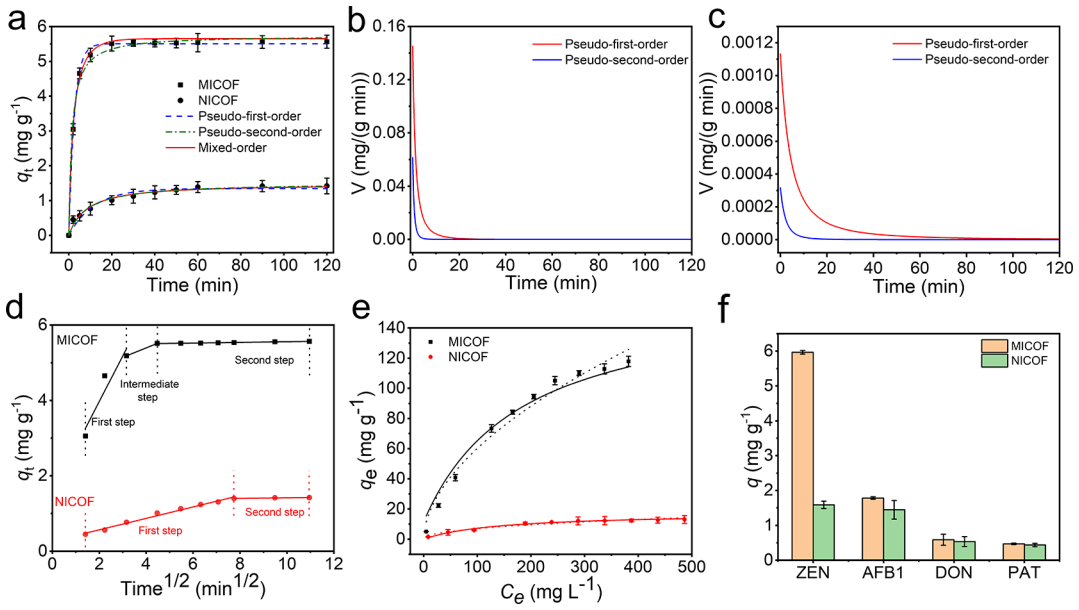

Figure 2. (a) Adsorption kinetics for ZEN (10 mL, 10 mg L^{-1}) on MICOF and NICOF (10 mg). (b) Mixed-order kinetics of MICOF toward ZEN. (c) Mixed-order kinetics for ZEN adsorption on NICOF. (d) Intraparticle diffusion model for ZEN adsorption on MICOF and NICOF. (e) Adsorption isotherms of ZEN (2 mL, 10−500 mg L^{-1}) on MICOF and NICOF (2 mg). Solid line and dashed line stand for the Langmuir and Freundlich model fitting, respectively. (f) Adsorption selectivity of MICOF and NICOF toward ZEN against AFB1, DON, and PAT (the initial concentrations of mycotoxins are 10 mg L^{-1}, solid/liquid = 2 mg/2 mL, time = 1 h).

in DOX and THF but poorly soluble in EtOH and ACN. The MICOF with the highly adsorption capacity and IF value was obtained in DOX (Figure S1c). In addition, the adsorption capacity and IF for ZEN of MICOF increased with the volume of DOX increasing and reached highest at 5 mL; thus, 5 mL of DOX was optimal (Figure S1d).

The type and amount of catalyst often affect the formation of COF. The most common catalyst used for the synthesis of imine-linked COF is HAc.[35] Therefore, we first examined HAc as the catalyst for the synthesis of MICOF at room temperature. Unfortunately, the MICOF prepared with HAc as the catalyst at room temperature gave low adsorption capacity and no imprinting effect for ZEN (Figure S8). We also tested the effect of HAc catalyst on the synthesis of MICOF by a traditional solvothermal synthesis method (120 °C, 3 days)[36] and found the obtained MICOF showed high crystallinity but still had no imprinting effect (Figure S9). This might be because high crystallinity COF tend to form ordered structures and are unable to form imprinted sites. Besides, $Sc(OTf)_3$ was also proposed to catalyze the fast fabrication of imine-linked COF at room temperature.[37] So, the effect of the amount of $Sc(OTf)_3$ on the adsorption performance of MICOF was studied (Figure S1e). The adsorption capacity of MICOF and IF value for ZEN first increased in the range of 1−6 mg $Sc(OTf)_3$ and then decreased when excessive catalyst was loaded (8−10 mg) due to fast reaction. Thus, 6 mg $Sc(OTf)_3$ was used for further work.

Polymerization reaction time is also an important factor on imprinting effect. As shown in Figure S1f, the imprinting effect was not obvious in the first 6 h of reaction although $Sc(OTf)_3$ can catalyze polymerization reaction rapidly, indicating that the imprinted sites were not fully formed. The specific adsorption increased with polymerization reaction time and reached the highest at 24 h.

Characterization of MICOF and NICOF. The as-prepared MICOF and NICOF were characterized by Fourier transform-infrared (FT-IR) spectroscopy, powder X-ray diffraction (PXRD) analysis, and scanning electron microscopy (SEM). A new bond at 1621 cm^{-1} in the FT-IR spectra of MICOF and NICOF confirms the imine bond formation (Figure S10a), indicating the successful synthesis of MICOF and NICOF. Both the as-prepared MICOF and NICOF were amorphous as indicated by the broad PXRD peaks (Figure S10b) likely due to the freedom orientation of building blocks and the lack of $\pi-\pi$ stacking.[34] A similar phenomenon was also observed in other molecularly imprinted COFs.[30] SEM images show the spherical morphology of both MICOF and NICOF (Figure S10c,d).

Adsorption Study. The adsorption kinetics of ZEN onto MICOF and NICOF were investigated by varying the adsorption time from 5 to 120 min with the initial ZEN concentration of 10 mg L^{-1} (Figure 2a). The adsorption kinetic parameters of MICOF and NICOF toward ZEN are listed and compared in Table S1. The MICOF showed faster adsorption kinetics (20 min for equilibrium) than the NICOF (60 min), due to the exposure of the imprinted sites of MICOF for adsorption.[31] The pseudo-first-order and pseudo-second-order kinetics models were used to fit ZEN adsorption kinetics (eqs S1−S3). The adsorption process on MICOF and NICOF were slightly better nonlinearly fitted by the pseudo-first-order kinetic model, and the corresponding theoretical equilibrium adsorption capacity (5.51 mg g^{-1} for MICOF and 1.34 mg g^{-1} for NICOF) was closer to the corresponding experimental value (5.56 mg g^{-1} for MICOF and 1.41 mg g^{-1} for NICOF). However, the pseudo-second-order kinetic model gave better linear fitting (Figure S11). The above results indicate that the actual adsorption processes are complex and often cannot be generalized. Therefore, the adsorption process was determined by the mixed-order kinetic model (eq S4).[38] The values of k_1' (the rate constant of pseudo-first-order, min^{-1}) and k_2' (the rate constant of pseudo-second-order, g mg^{-1} min^{-1}) were obtained by the mixed-order kinetic model,

https://doi.org/10.1021/acs.analchem.3c05512
Anal. Chem. 2024, 96, 3561−3568

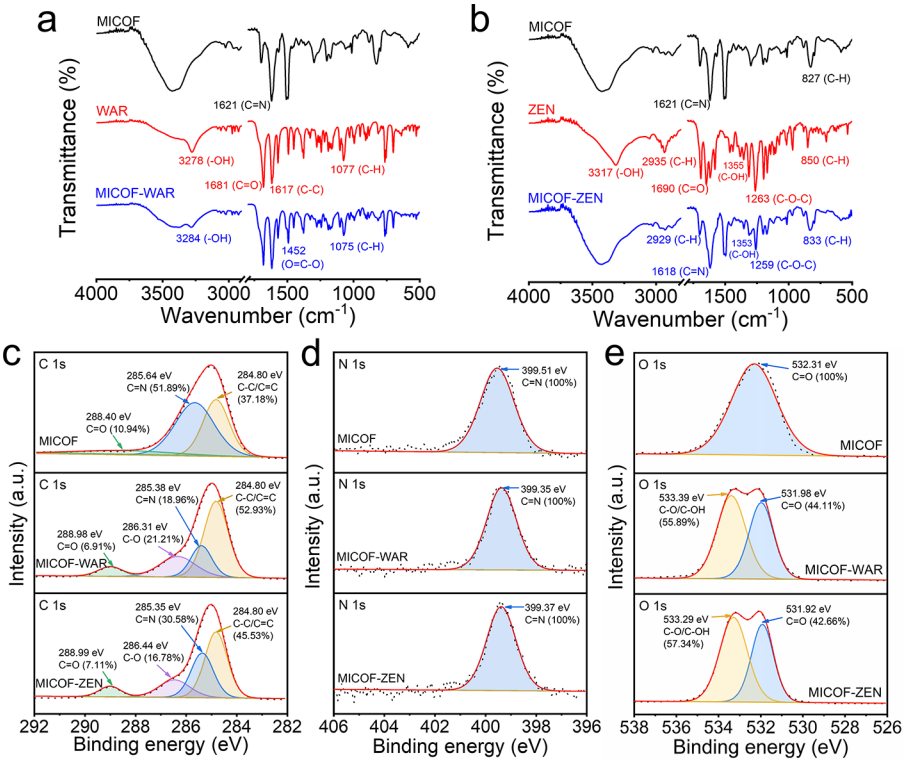

Figure 3. (a) FT-IR spectra of MICOF, WAR, and MICOF−WAR. (b) FT-IR spectra of MICOF, ZEN, and MICOF−ZEN. Deconvolution analysis of C 1s (c), N 1s (d), and O 1s (e) XPS spectra of MICOF, MICOF−WAR, and MICOF−ZEN (dashed lines: raw curves, red lines: fitting curves).

indicating that the adsorption process included pseudo-first-order and pseudo-second-order kinetics. Specifically, the contributions of two kinetics model rates in the adsorption process of MICOF and NICOF are presented in Figure 2b,c. The pseudo-first-order rate was around three times higher than the pseudo-second-order rate at the initial stage of adsorption. At a certain time (5 min for MICOF and 10 min for NICOF), the pseudo-second-order kinetic rate decreased to almost zero. Then, the pseudo-first-order rate continuously decreased until the adsorption equilibrium. Therefore, we can conclude that the adsorption of ZEN on MICOF was coparticipated by both the pseudo first-order and second-order kinetic processes, but dominated by a pseudo-first-order kinetic process. In addition, MICOF showed faster adsorption (larger k value) than NICOF (Table S1).

The intraparticle diffusion model was also applied to elucidate the diffusion process of ZEN on MICOF and NICOF. Plots of q_t against $t^{1/2}$ were obtained (Figure 2d), and the corresponding kinetic parameters were calculated (Table S1). The q_t−$t^{1/2}$ plots show multilinear graph while the fitting lines did not pass through the origin, suggesting that the intraparticle diffusion is not the sole rate-controlling step. In this case, the adsorption process of ZEN onto the sorbents occurs through two main steps: ZEN diffused into the external surface of sorbents (Step 1) and into the micropore of the sorbents to reach the equilibrium (Step 2). As shown in Figure 2d, the MICOF showed faster adsorption than the NICOF in Step 1. Moreover, an additional intermediate step was observed for the MICOF, which is the characteristic of ZEN transport within the inner surface of MICOF before the adsorption equilibrium.[39] This phenomenon suggests that the imprinted sites of MICOF were involved in this intermediate adsorption process.

We further applied Langmuir and Freundlich models to analyze the adsorption isotherms (Figures 2e and S12). The Langmuir model gave better fitting than Freundlich model, indicating ZEN adsorption onto MICOF is monolayer with a limited adsorption site.[40] The theoretical maximum sorption capacities of ZEN on MICOF and NICOF were 177.2 and 17.5 mg g^{-1}, respectively, giving the IF value of 10.1 (Table S2). The separation factor (R_L) of MICOF and NICOF, which is usually used to determine if the adsorption is favorable ($0 < R_L < 1$) or not ($R_L > 1$),[41] were calculated to be 0.2667−0.9479 and 0.2198−0.9337, respectively (Table S2), indicating a favorable adsorption of ZEN by MICOF and NICOF. The intensity factor $1/n$ indicates the intensity of adsorption ($1/n$ between 0−1 means favorable adsorption).[42] The $1/n$ values for MICOF and NICOF were 0.55 and 0.45, respectively (Table S2), indicating the favorable adsorption of ZEN on both adsorbents. The distribution coefficient value (K_d) can measure the affinity of sorbent to target. The K_d of MICOF was 1029 mL g^{-1}, 25 times higher than that of NICOF (42 mL g^{-1}) (Table S2), suggesting that the MICOF has much higher affinity than NICOF to ZEN.

Adsorption selectivity is the key issue for molecularly imprinted polymers. To demonstrate the selectivity of MICOF to ZEN, the adsorption of three other mycotoxins (AFB1, DON and PAT) on MICOF were also studied for comparison. The adsorption capacity of MICOF for ZEN was significantly higher than those for other three mycotoxins (Figure 2f). The distribution coefficient (K_d, L g^{-1}) for ZEN, AFB1, DON, and PAT, the selectivity coefficient (K), and relative selectivity coefficient (K') for ZEN to AFB1, DON, and PAT were

https://doi.org/10.1021/acs.analchem.3c05512
Anal. Chem. 2024, 96, 3561−3568

calculated based on eqs S8−S10.[43] The results are summarized in Table S3. MICOF gave much larger K_d value toward ZEN (1.48 L g^{-1}) than other mycotoxins (0.05−0.22 L g^{-1}). Furthermore, the K' values for ZEN to AFB1, DON, and PAT were 6.0, 7.8, and 7.8, respectively, showing MICOF possessed superior adsorption selectivity toward ZEN.

The adsorption capacity of MICOF for ZEN was studied under different pH (Figure S13a). At pH 4−5, MICOF gave the relatively low adsorption capacity for ZEN. When pH < pK_a (7.58 for ZEN), the ZEN exists predominantly in the form of cations with C=OH^+ groups,[44] the MICOF is also positively charged (Figure S13b). At pH 6−8, MICOF gave the high adsorption capacity due to the weakness of electrostatic repulsion between ZEN and MICOF. At pH 9, the ZEN mainly exists in the form of anion with C=O^- groups,[45] and MICOF is also negatively charged, so the adsorption capacity slightly reduced.

Adsorption Interaction. The interaction between the functional monomer and the template or analyte plays a crucial role in the formation of an imprinted cavity of MIP or the rebinding of the analyte to MIP.[22] Here, the interaction of MICOF with WAR and ZEN was explored by FT-IR and X-ray photoelectron spectroscopy (XPS).

Figure 3a,b show the FT-IR spectra of pure WAR and ZEN and MICOF after and before adsorption. The −OH stretching (from 3278 to 3284 cm^{-1}) of WAR, C−OH in-plane bending vibration (from 1355 to 1353 cm^{-1}) of ZEN, C=N stretching (from 1621 to 1618 cm^{-1}) of MICOF were shifted after adsorption, due to the hydrogen bond interaction (C−OH···N=C) between target molecule and MICOF.[46] Meanwhile, the C−H in-plane bending vibration of WAR at 1077 cm^{-1} slightly moved to 1075 cm^{-1}. As for ZEN, the out-plane bending vibration and asymmetric stretching of C−H shifted from 2935 to 2929 cm^{-1}, and from 850 to 833 cm^{-1}, respectively, as the result of the $\pi-\pi$ interaction between target molecule and MICOF.[47]

The XPS spectra of the MICOF before and after the adsorption of WAR and ZEN are compared (Figures 2c−e, S14, and S15). New C 1s and O 1s peaks for C−O/C−OH appeared in MICOF after the adsorption of WAR and ZEN (Figures 2c,e and S15).[48] Moreover, the peaks of O 1s for C−O/C−OH changed from 533.25 and 532.78 eV to 533.39 and 533.29 eV in WAR and ZEN after their adsorption on MICOF, respectively. The characteristic peaks of C 1s for C=N of imine linkage of MICOF shifted from 285.64 eV to 285.38 and 285.35 eV (Figure 3c), and the binding energy of N 1s for C=N changed from 399.51 eV to 399.35 and 399.37 eV after the adsorption of WAR and ZEN, respectively (Figure 3d).[49] The above results also show the presence of hydrogen bonding (C−OH···N=C) in MICOF with WAR and ZEN.

Selectivity and Reusability of MICOF. Other mycotoxins with the same spiked concentration were added to the extraction process to investigate the selectivity of MICOF for ZEN. As shown in Figure S16, the recovery of ZEN was not affected by other mycotoxins (over 97% for all), which again confirmed the high selectivity of MICOF for ZEN.

The regeneration is the important index to investigate the performance of the adsorbent. After five cycles of extraction-elution, MICOF still gave over 92% recovery for ZEN (Figure S17). The FI-IR spectra and PXRD pattern (Figure S18) of the fresh and regenerated MICOF showed no obvious change. The above results prove that MICOF has good reusability.

Analytical Performance. Under the optimized DSPE conditions (Figure S19), the calibration curves were constructed by using ZEN-free cereals extracts standard addition method. Calibration curves were obtained in standard solution and in different sample matrixes (Figure S20). The coefficients of determination (R^2) ranged from 0.9996 to 0.9999. The ratios of the sensitivity in sample matrix to that in standard solution were calculated in the ranged of 0.9719−0.9997 (Table S4), while t test also revealed no significant difference between the sensitivity in sample matrix and that in standard solution ($0.14 < P < 0.65$) (Table S4). These results indicate negligible matrix effect due to high selectivity of the developed MICOF for ZEN extraction. This remarkable advantage of the developed method allows the use of a simple standard curve calibration for the quantitation of ZEN in real samples. The limits of detection (LOD, S/N = 3) and quantification (LOQ, S/N = 10) were 0.21 and 0.70 $\mu g\ kg^{-1}$, respectively, which are considerably lower than the maximum residue limits in the range of 20−400 $\mu g\ kg^{-1}$ (specified by European Commission). The intra- and inter-day relative standard deviation (RSD, $n = 6$) for the determination of ZEN were in the ranges of 1.2−1.8% and 2.4−3.8% respectively (Table S5).

The developed method was compared with other reported methods in terms of linear range, detection limit, recovery and precision (Table S6). Our method shows the lower detection limit, higher accuracy, higher precision and wider linear range than other reported methods. In addition, the as-prepared MICOF gave larger adsorption capacity and higher selectivity than other MIPs for ZEN.

The developed method was further validated by analyzing a certified reference material MRM-ZW-02030 (wheat). The content of ZEN determined by the developed method using a simple standard curve calibration (297.8 ± 6.9 $\mu g\ kg^{-1}$) is in good agreement with the certified content (311.7 ± 40 $\mu g\ kg^{-1}$), indicating the good accuracy of the developed method.

Application to Real Samples. The developed method was applied to the analysis of real cereal samples including rice, millet, wheat, oat and maize for ZEN using a simple standard curve calibration. As shown in Tables 1 and S7, the absolute recoveries for the spiked ZEN in the concentration range of 50−200 $\mu g\ kg^{-1}$ in these samples ranged from 93.7 to 101.4%. Among the five real samples analyzed, ZEN was only found in maize sample (2.7 ± 0.1 $\mu g\ kg^{-1}$, Figure S21).

CONCLUSIONS

We have reported a simple room temperature fabrication of MICOF for selective extraction of ZEN in complex food samples. A pore size adjustment strategy for the design of MICOF and a rational consideration for the select of pseudo-template have been proposed to achieve high selectivity of MICOF. The as-synthesized MICOF gives the largest adsorption capacity and highest imprinting factor for the extraction of ZEN so far. The MICOF has been successfully employed as the DSPE sorbent for HPLC determination of ZEN. The high selectivity of the MICOF allows matrix effect-free determination of ZEN in real samples. The developed method shows lower detection limit, higher accuracy, higher precision, and wider linear range than other reported methods. The proposed strategy can be extended to the fabrication of MICOF for select extraction of other hazardous compounds by rational selecting pseudo-template in conjunction with

https://doi.org/10.1021/acs.analchem.3c05512
Anal. Chem. 2024, 96, 3561−3568

Table 1. Analytical Results for Real Samples Using the Developed Method

sample	spiked ZEN ($\mu g\ kg^{-1}$)	concentration determined ($\mu g\ kg^{-1}$, mean ± s,n = 6)	absolute recovery (%, mean ± s,n = 6)
rice 1	0	ND[a]	
	50	47.9 ± 1.2	95.9 ± 2.5
	100	94.5 ± 1.6	94.5 ± 1.6
	200	195.2 ± 2.8	97.6 ± 1.4
millet 1	0	ND	
	50	46.9 ± 0.3	93.7 ± 0.6
	100	94.2 ± 0.9	94.2 ± 0.9
	200	187.9 ± 1.4	94.0 ± 0.7
wheat 1	0	ND	
	50	49.5 ± 0.9	99.0 ± 1.9
	100	101.4 ± 1.6	101.4 ± 1.6
	200	202.5 ± 3.5	101.3 ± 1.8
oat 1	0	ND	
	50	49.1 ± 1.4	96.0 ± 2.8
	100	97.5 ± 3.2	97.5 ± 3.2
	200	199.3 ± 2.9	99.6 ± 1.4
maize 1	0	2.7 ± 0.1	
	50	51.2 ± 1.3	97.2 ± 2.5
	100	98.6 ± 1.8	96.0 ± 1.8
	200	194.2 ± 3.1	95.8 ± 1.5

[a]ND, not detected.

controlling the length of the linker to adjust the pore size of MICOF.

■ ASSOCIATED CONTENT

Supporting Information

The Supporting Information is available free of charge at https://pubs.acs.org/doi/10.1021/acs.analchem.3c05512.

All experimental material and more experimental details and results, including characterization apparatus, adsorption isotherms, and kinetic model equations; structural formula of zearalenone and its analogues; molecular docking study; SEM images; FT-IR spectra; XRD patterns; N_2 adsorption−desorption isotherms of MICOF and NICOF; and optimization of DSPE (PDF)

■ AUTHOR INFORMATION

Corresponding Author

Xiu-Ping Yan − *State Key Laboratory of Food Science and Resources, Jiangnan University, Wuxi 214122, China; International Joint Laboratory on Food Safety, Institute of Analytical Food Safety, School of Food Science and Technology, and Key Laboratory of Synthetic and Biological Colloids, Ministry of Education, School of Chemical and Material Engineering, Jiangnan University, Wuxi 214122, China;* orcid.org/0000-0001-9953-7681; Email: xpyan@jiangnan.edu.cn

Authors

Hao-Ze Li − *State Key Laboratory of Food Science and Resources, Jiangnan University, Wuxi 214122, China; International Joint Laboratory on Food Safety and Institute of Analytical Food Safety, School of Food Science and Technology, Jiangnan University, Wuxi 214122, China*

Cheng Yang − *State Key Laboratory of Food Science and Resources, Jiangnan University, Wuxi 214122, China; International Joint Laboratory on Food Safety and Institute of Analytical Food Safety, School of Food Science and Technology, Jiangnan University, Wuxi 214122, China*

Hai-Long Qian − *State Key Laboratory of Food Science and Resources, Jiangnan University, Wuxi 214122, China; International Joint Laboratory on Food Safety and Institute of Analytical Food Safety, School of Food Science and Technology, Jiangnan University, Wuxi 214122, China;* orcid.org/0000-0001-7554-4115

Shu-Ting Xu − *State Key Laboratory of Food Science and Resources, Jiangnan University, Wuxi 214122, China; International Joint Laboratory on Food Safety and Institute of Analytical Food Safety, School of Food Science and Technology, Jiangnan University, Wuxi 214122, China*

Complete contact information is available at: https://pubs.acs.org/10.1021/acs.analchem.3c05512

Notes

The authors declare no competing financial interest.

■ ACKNOWLEDGMENTS

This work was supported by the National Natural Science Foundation of China (no. 22176073) and the Program of "Collaborative Innovation Center of Food Safety and Quality Control in Jiangsu Province".

■ REFERENCES

(1) Leite, M.; Freitas, A.; Silva, A. S.; Barbosa, J.; Ramos, F. *Trends Food Sci. Technol.* **2021**, *115*, 307−331.

(2) Catteuw, A.; Broekaert, N.; De Baere, S.; Lauwers, M.; Gasthuys, E.; Huybrechts, B.; Callebaut, A.; Ivanova, L.; Uhlig, S.; De Boevre, M.; et al. *J. Agric. Food Chem.* **2019**, *67*, 3448−3458.

(3) Wu, K.; Ren, C.; Gong, Y.; Gao, X.; Rajput, S. A.; Qi, D.; Wang, S. *Anim. Nutr.* **2021**, *7*, 587−594.

(4) Peters, J.; Ash, E.; Gerssen, A.; Van Dam, R.; Franssen, M. C. R.; Nielen, M. W. F. *Toxins* **2021**, *13*, 366.

(5) Ropejko, K.; Twarużek, M. *Toxins* **2021**, *13*, 35.

(6) Zhang, Y.; Liu, D.; Peng, J.; Cui, Y.; Shi, Y.; He, H. *Talanta* **2020**, *209*, No. 120555.

(7) Huang, Z.; He, J.; Li, H.; Zhang, M.; Wang, H.; Zhang, Y.; Li, Y.; You, L.; Zhang, S. *Food Chem.* **2020**, *308*, No. 125696.

(8) Han, Z.; Jiang, K.; Fan, Z.; Diana Di Mavungu, J.; Dong, M.; Guo, W.; Fan, K.; Campbell, K.; Zhao, Z.; Wu, Y. *Food Control* **2017**, *79*, 177−184.

(9) Qian, M.; Zhang, H.; Wu, L.; Jin, N.; Wang, J.; Jiang, K. *Food Chem.* **2015**, *166*, 23−28.

(10) De Rycke, E.; Foubert, A.; Dubruel, P.; Bol'hakov, O. I.; De Saeger, S.; Beloglazova, N. *Food Chem.* **2021**, *353*, No. 129342.

(11) Hendrickson, O. D.; Chertovich, J. O.; Zherdev, A. V.; Sveshnikov, P. G.; Dzantiev, B. B. *Food Control* **2018**, *84*, 330−338.

(12) Jiang, K.; Huang, Q.; Fan, K.; Wu, L.; Nie, D.; Guo, W.; Wu, Y.; Han, Z. *Food Chem.* **2018**, *264*, 218−225.

(13) Khalifehzadeh, E.; Ahmadi, S.; Beigmohammadi, F. *Microchem. J.* **2021**, *170*, No. 106682.

(14) Pochivalov, A.; Pavlova, K.; Garmonov, S.; Bulatov, A. *J. Mol. Liq.* **2022**, *366*, No. 120331.

(15) Macías-Montes, A.; Rial-Berriel, C.; Acosta-Dacal, A.; Henríquez-Hernández, L. A.; Almeida-González, M.; Rodríguez-Hernández, Á.; Zumbado, M.; Boada, L. D.; Zaccaroni, A.; Luzardo, O. P. *Sci. Total Environ.* **2020**, *708*, No. 134592.

(16) Huang, Z.; He, J.; Li, Y.; Wu, C.; You, L.; Wei, H.; Li, K.; Zhang, S. *J. Chromatogr. A* **2019**, *1602*, 11−18.

(17) Büyüktiryaki, S.; Keçili, R.; Hussain, C. M. *Trend. Anal. Chem.* **2020**, *127*, No. 115893.

(18) Du, L.-J.; Chu, C.; Warner, E.; Wang, Q.-Y.; Hu, Y.-H.; Chai, K.-J.; Cao, J.; Peng, L.-Q.; Chen, Y.-B.; Yang, J.; et al. *J. Chromatogr. A* **2018**, *1561*, 1−12.

(19) González-Sálamo, J.; Socas-Rodríguez, B.; Hernández-Borges, J.; Rodríguez-Delgado, M. Á. *Food Chem.* **2017**, *215*, 362−368.
(20) Thongprapai, P.; Cheewasedtham, W.; Chong, K. F.; Rujiralai, T. *J. Sep. Sci.* **2018**, *41* (23), 4348−4354.
(21) Arabi, M.; Ostovan, A.; Li, J.; Wang, X.; Zhang, Z.; Choo, J.; Chen, L. *Adv. Mater.* **2021**, *33*, No. 2100543.
(22) BelBruno, J. J. *Chem. Rev.* **2019**, *119*, 94−119.
(23) Chen, L.; Wang, X.; Lu, W.; Wu, X.; Li, J. *Chem. Soc. Rev.* **2016**, *45*, 2137−2211.
(24) Du, Q.; Wu, P.; Hu, F.; Li, G.; Shi, J.; He, H. *New J. Chem.* **2019**, *43*, 7044−7050.
(25) Zhao, Q.; Zhang, H.; Zhao, H.; Liu, J.; Liu, J.; Chen, Z.; Li, B.; Liao, X.; Regenstein, J. M.; Wang, J.; et al. *ACS Appl. Mater. Interfaces* **2020**, *12*, 8751−8760.
(26) Diercks, C. S.; Yaghi, O. M. *Science* **2017**, *355*, No. eaal1585.
(27) Li, H.-Z.; Yang, C.; Qian, H.-L.; Yan, X.-P. *Sep. Purif. Technol.* **2023**, *306*, No. 122704.
(28) Zhai, Y.; Bao, Y.; Ning, T.; Chen, P.; Di, S.; Zhu, S. *J. Chromatogr. A* **2023**, *1692*, No. 463850.
(29) Wang, W.; Liu, T.; Wang, Y.; Mu, G.; Zhang, F.; Yang, Q.; Hou, X. *J. Agric. Food Chem.* **2022**, *70*, 12211−12219.
(30) Li, C.-Y.; Lv, S.-W.; Yang, L.; Wang, J.; Liu, J.-M.; Wang, S. *J. Hazard. Mater.* **2022**, *438*, No. 129566.
(31) Ji, W.; Sun, R.; Geng, Y.; Liu, W.; Wang, X. *Anal. Chim. Acta* **2018**, *1001*, 179−188.
(32) Zhao, Q.; Zhang, H.; Zhao, H.; Zhu, H.; Liu, J.; Li, B.; Li, M.; Yang, X. *J. Agric. Food Chem.* **2023**, *71*, 18024−18036.
(33) Guan, X.; Chen, F.; Fang, Q.; Qiu, S. *Chem. Soc. Rev.* **2020**, *49*, 1357−1384.
(34) Guan, X.; Chen, F.; Qiu, S.; Fang, Q. *Angew. Chem., Int. Ed. Engl.* **2022**, No. e202213203.
(35) Smith, B. J.; Overholts, A. C.; Hwang, N.; Dichtel, W. R. *Chem. Commun.* **2016**, *52*, 3690−3693.
(36) Uribe-Romo, F. J.; Hunt, J. R.; Furukawa, H.; Klock, C.; O'Keeffe, M.; Yaghi, O. M. *J. Am. Chem. Soc.* **2009**, *131*, 4570−4571.
(37) Matsumoto, M.; Dasari, R. R.; Ji, W.; Feriante, C. H.; Parker, T. C.; Marder, S. R.; Dichtel, W. R. *J. Am. Chem. Soc.* **2017**, *139*, 4999−5002.
(38) Guo, X.; Wang, J. *J. Mol. Liq.* **2019**, *288*, No. 111100.
(39) Álvarez-Torrellas, S.; Rodríguez, A.; Ovejero, G.; García, J. *Chem.Eng. J.* **2016**, *283*, 936−947.
(40) Cheng, G.; Li, X.; Li, X.; Chen, J.; Liu, Y.; Zhao, G.; Zhu, G. *J. Hazard. Mater.* **2022**, *423*, No. 127087.
(41) Farrukh, A.; Akram, A.; Ghaffar, A.; Hanif, S.; Hamid, A.; Duran, H.; Yameen, B. *ACS Appl. Mater. Interfaces* **2013**, *5*, 3784−3793.
(42) Nayab, S.; Farrukh, A.; Oluz, Z.; Tuncel, E.; Tariq, S. R.; Ur Rahman, H.; Kirchhoff, K.; Duran, H.; Yameen, B. *ACS Appl. Mater. Interfaces* **2014**, *6*, 4408−4417.
(43) Cui, Y.; Kang, W.; Qin, L.; Ma, J.; Liu, X.; Yang, Y. *Chem. Eng. J.* **2020**, *397*, No. 125480.
(44) Qian, H. L.; Meng, F. L.; Yang, C. X.; Yan, X. P. *Angew. Chem., Int. Ed. Engl.* **2020**, *59*, 17607−17613.
(45) Mo, P.; Fu, D.; Chen, P.; Zhang, Q.; Zheng, X.; Hao, J.; Zhuang, X.; Liu, H.; Liu, G.; Lv, W. *Sep. Purif. Technol.* **2021**, *278*, No. 119238.
(46) Zhao, R.; Zheng, H.; Zhong, Z.; Zhao, C.; Sun, Y.; Huang, Y.; Zheng, X. *Sci. Total Environ.* **2021**, *760*, No. 144307.
(47) Xu, H.; Zhu, S.; Xia, M.; Wang, F. *J. Hazard. Mater.* **2021**, *402*, No. 123815.
(48) Feng, J.-B.; Li, Y.-Y.; Zhang, Y.; Xu, Y.-Y.; Cheng, X.-W. *Chem. Eng. J.* **2022**, *429*, No. 132499.
(49) Li, X.; Qi, Y.; Yue, G.; Wu, Q.; Li, Y.; Zhang, M.; Guo, X.; Li, X.; Ma, L.; Li, S. *Green Chem.* **2019**, *21*, 649−657.

https://doi.org/10.1021/acs.analchem.3c05512
Anal. Chem. 2024, 96, 3561−3568